PEC: Synthetic Aperture RFID Localization with Aperture Position Error Compensation

Run Zhao*, Dong Wang†, Qian Zhang†, Haonan Chen† and Huatao Xu†
*Department of Computer Science and Engineering, Shanghai Jiao Tong University, China; Email: zhaorun@cs.sjtu.edu.cn
†School of Software, Shanghai Jiao Tong University, China; Email:{wangdong, qwert3472, chn, xuhuatao}@sjtu.edu.cn

***Abstract*—In recent years, location-based services have been widely applied not only in daily life but also in automation industries. As one of main location sensing technologies, RFID based localization has attracted increasing attention. Existing synthetic aperture RFID localization systems use the inverse correlation filter to reconstruct holograms and achieve satisfactory accuracy. However, these methods require accurate aperture positions for theoretical signal construction, while the ubiquitous aperture uncertainty in practice causes non-negligible performance degradation. In this paper, we present PEC, an accurate synthetic aperture RFID localization system with aperture position error compensation, which has a major advantage over the classic systems for no need to know the exact trajectory of the synthetic aperture. We first build a mathematical model for localization and merge all coherent received signals to estimate the tag position. Then we propose an iterative algorithm which can alternately estimate both the tag position and the aperture position error. We have implemented and evaluated PEC using commercial-off-the-shelf (COTS) RFID devices. Extensive experimental results show that it achieves the cm-level accuracy with aperture position error in noisy environments, which proves its effectiveness and robustness.**

***Index Terms*—RFID, Localization, Aperture Position Error Compensation**

I. Introduction

The integration with information technology like Internet of Things revolutionizes manufacturing industry worldwide, such as Industrial Internet and Industry 4.0, changing the way of producing and moving goods in factories and warehouses. Radio Frequency Identification (RFID) tags have been widely deployed in intelligent factories as important information carriers [1], [2]. Meanwhile, Automated Guided Vehicle (AGV) is introduced to reduce manual work with high flexibility and low installation cost especially in intelligent manufacturing and flexible manufacturing. AGV equipped with an RFID reader needs to perform complex tasks, such as searching and locating the desired object attached with RFID tags, picking it up and delivering it to the destination workstation or assembly line with autonomous navigation capability, all of which require cm-level localization accuracy [1], [3].

Indoor robot or AGV localization and navigation have been arousing great interests in both the academia and industry recently. Some encouraging systems are proposed but with restrictions in practice. Vision or Laser based systems [4] achieve high accuracy with strong dependence on light or line-of-sight (LOS) and may arouse serious privacy concerns. AGV using magnetic tape or inductive wire based navigation [5] is limited by the track. Inertial navigation systems [6] usually have serious accumulated errors, and other wireless signal based localization systems are open to interference [7], [8]. These existing systems cannot perfectly satisfy the demand in intelligent manufacturing for low-cost, effective, and easy-to-deploy localization, as well as applicability in bad lighting and NLOS (non-line-of-sight) scenarios.

Passive RFID tags, benefiting from its wireless, inexpensive and battery-free sensing ability [9], have been extensively applied in indoor localization applications. The state-of-the-art RFID localization methods are incorporating with Synthetic Aperture Radar (SAR) technology to open up endless potential for better localization performance. These synthetic aperture RFID localization systems [9]–[16] usually leverage the relative motion between the reader antenna and the tag and achieve cm-level accuracy. With the synthetic aperture RFID localization technology, the AGV with the RFID reader can not only identify and locate target objects attached with tags, but also achieve self-positioning using a few reference tags, which is a dual problem of the tag localization.

One limitation of these systems is that they need to know the accurate aperture position. For each possible target position, they leverage the inverse correlation filter between measured signals and corresponding theoretical signals to reconstruct the likelihood, while these theoretical ones are determined by aperture positions [13]. Their performance will degrade significantly in the presence of the aperture position error (the gap between the known aperture position and the actual one) due to the distorted theoretical signal. As shown in Fig. 1, with a greater accumulated error along the aperture, the estimated position of the synthetic aperture RFID localization technology increasingly deviates away from the actual one. Furthermore, noise and other interference in practice will also result in performance degradation.

Unfortunately, the aperture position error is very common for moving platforms without sophisticated sensors. To address this issue, Mobitagbot [13] assumes the speed and speed drift to be constant for calibration. This assumption is applicable for slow robots moving at a constant speed (0.05 m/s), while it does not hold for faster AGVs, of which the acceleration and deceleration are not negligible. The motion compensation used for airborne or spaceborne SAR [17]–[19] usually simplify the relative motion model, or focus on the phase error, or take hundreds of seconds to compensate for phase distortions.

Toward these ends, we propose PEC, a synthetic aperture

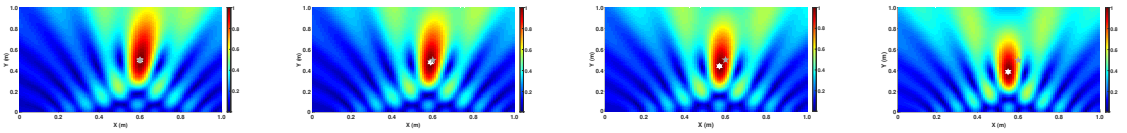

(a) 0 m (0.6 m, 0.5 m). (b) 0.025 m (0.59 m, 0.48 m). (c) 0.05 m (0.57 m, 0.44 m). (d) 0.1 m (0.55 m, 0.39 m).

Fig. 1. Holograms with different accumulated error along the aperture. (The pentagram is the actual position (0.6 m, 0.5 m) and hexagram means the estimated position. The title of each subfigure is the accumulated error, e.g. 0.1 m in (d) means that the accumulated error increases from 0 (the first aperture point) to 0.1 m (the last aperture point). There are 21 aperture points with uniform spacing from (0, 0) to (1 m, 0).)

RFID localization method with aperture position error compensation. The challenges and solutions are as follows:

(1) *How to compensate for the aperture position error?* A straightforward idea is to traverse all possible aperture positions like the hologram, but it is impractical to construct phase profiles for all possible positions due to exponential time complexity. Instead, PEC abstracts the localization as an optimization problem, described by a localization model, in which the aperture position error and the tag position are independent. The proposed model directly uses the aperture position error without any approximations, which can account for any measurement method of a relative trajectory. On the basis of deliberating over the factors that dominate phase changes, the tag position and aperture error are alternately estimated by an iterative algorithm. In the second step of each iteration, the aperture position error is calculated by solving a set of unconstrained optimization problems.

(2) *How to estimate the target tag position accurately?* Unlike existing synthetic aperture RFID localization systems, PEC uses reflection coefficients instead of likelihood obtained with the inverse correlation filter to represent the target tag position. PEC takes full advantage of reported phase at different points and different carrier frequencies and merges them coherently. Inspired by radar imaging, we introduce compressed sensing to estimate the reflection coefficients for tag localization. Moreover, the relative phase and phase calibration are utilized to improve the localization performance.

In summary, we have the following contributions: To the best of our knowledge, PEC is the first synthetic aperture RFID localization method with aperture position error compensation. We propose a localization model in consideration of aperture position error and formulate the localization problem as an optimization problem, which is solved by an iteration algorithm. We build a prototype of PEC using COTS RFID devices, and extensive experimental results prove its effectiveness and robustness with an average localization accuracy of 0.05 m.

The remainder of this paper is organized as follows. At first, Section II presents the localization model. In Section III, the detailed designs of PEC are proposed. Then Section IV demonstrates the evaluation of PEC. We review the related works in Section V. Finally, Section VI concludes this paper.

II. PEC Localization Model

Present COTS RFID readers can report the phase value φ, which includes three components [20]:

$$\varphi = (\varphi_{prop} + \varphi_{\mathrm{r}} + \varphi_{\mathrm{t}}) \mod 2\pi, \tag{1}$$

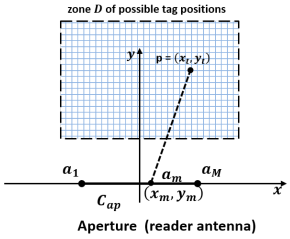

Fig. 2. Synthetic aperture RFID localization. (The midpoint of C_{ap} is set as the coordinate origin, and the direction of motion is the x-direction.)

where $\varphi_{prop} = 4\pi d/\lambda$ is the phase rotation due to the signal propagation in the space (λ is the carrier wavelength, and $2d$ is the propagation distance), while φ_{r} and φ_{t} denote the phase accumulated by the reader antenna and tag respectively. φ_{t} can be deemed as a constant for one tag, whereas φ_{r} is frequency-dependent. Due to a fundamental limit, φ repeats when the distance d changes every $\lambda/2$ and it can not be unwrapped without ambiguity, leading to ambiguous estimated distance.

The synthetic aperture RFID localization leverages coherence of reported phase at different aperture points to deal with this ambiguity. Its geometric model with a linear aperture is depicted in Fig. 2. The reader antenna moves along C_{ap}, known as the synthetic aperture, and interrogates a static tag $\mathbf{p}$ at aperture points $\mathbf{a}_m$. The attenuation and φ_{t} caused by the tag is recorded as its reflection coefficient r, so the received signal is $r\exp\{-j(4\pi d/\lambda+\varphi_{\mathrm{r}})\}$, where the received signal strength is neglected due to its coarse-grain and instability [12].

Evidently, the possible tag position is in the RFID interrogation zone and is also limited by some deployment constraints. Unlike existing RFID localization methods, we regard all possible tag positions (zone D) as a whole to reflect the signal, which is similar to the synthetic aperture radar imaging [19]. An RFID reader can only successfully demodulate the signal reflected from the interrogated tag at one time point [21]. Accordingly, the received signal can be viewed as the cumulative sum of reflected signals from all points with respective r, and only the reflection coefficient corresponding to the actual tag position is non-zero.

The zone D is partitioned into $P \times Q$ grids to represent possible tag positions for convenience, which can be expressed by a $PQ \times 1$ reflection coefficients vector $\mathbf{r}$:

$$\mathbf{r} = [r(1,1), ..., r(1,Q), ..., r(p,q), ..., r(P,Q)]^T \tag{2}$$

where $r(p,q)$ is the reflection coefficient of the grid in p^{th}

row and q^{th} column of the discrete zone D.

Most UHF RFID readers use frequency hopping spread spectrum [21], which means the reported phase at different aperture points may have respective carrier frequencies. If the carrier frequency index of aperture point $\mathbf{a}_m$ is recorded as n_m, the ideal received signals along the aperture can be written as an $M \times 1$ column vector $\hat{\mathbf{s}} = [\hat{s}(1), ..., \hat{s}(M)]^T$:

$$\hat{s}(m) = \sum_{i=1}^{PQ} \mathbf{r}(i) \exp\left\{-j\left[\frac{4\pi d(m,i)}{\lambda_{n_m}} + \varphi_{n_m,\mathrm{r}}\right]\right\} \quad (3)$$

where $\mathbf{r}(i)$ is the reflection coefficient of the i^{th} grid, $d(m,i)$ is the distance between this grid and $\mathbf{a}_m$, and λ_{n_m} is the corresponding wavelength. The unique non-zero element of $\mathbf{r}$ represents the tag position, so the localization problem is to find the non-zero $\mathbf{r}(i)$. In the space, different points suffer different ambient noises and multi-path effects [22]. Those distortions will weaken each other in the position estimation with the dissimilar reported phase at different aperture points.

The received signal s along the aperture can also be written as a vector $\mathbf{s} = [s(1), ..., s(M)]^T$, which are supposed to be equal to the ideal one $\hat{\mathbf{s}}$. Therefore, all received signals $\mathbf{s}$ can be expressed as $\mathbf{s} = \mathbf{A}\mathbf{r}$ in the form of matrix, where the $M \times PQ$ measurement matrix $\mathbf{A}$ expresses the relationship between the reflection coefficients $\mathbf{r}$ and the measured signals $\mathbf{s}$. The elements of $\mathbf{s}$ and $\mathbf{A}$ can be calculated by (4):

$$\begin{aligned} s(m) &= \exp\{-j\varphi_m\}, \\ a(m,i) &= \exp\left\{-j\left[\frac{4\pi d(m,i)}{\lambda_{n_m}} + \varphi_{n_m,\mathrm{r}}\right]\right\} \end{aligned} \quad (4)$$

where φ_m is the reported phase at aperture point $\mathbf{a}_m$, and $a(m,i)$ is the theoretical signal reflected from the i^{th} grid to the antenna at $\mathbf{a}_m$ without the reflection coefficient $\mathbf{r}(i)$. With a noise vector $\mathbf{n}$ as the error correction term, the synthetic aperture RFID localization model is:

$$\mathbf{s} = \mathbf{A}\mathbf{r} + \mathbf{n} \quad (5)$$

As mentioned before, it is usually difficult to get the exact aperture position in real situation, but $\mathbf{A}$ depends on the aperture position, and the aperture position error will result in the uncertainty of $\mathbf{A}$. For example, the position of aperture point $\mathbf{a}_m$ is known as (x_m, y_m), while its actual position is $(x_m + \Delta x_m, y_m + \Delta y_m)$, where Δx_m and Δy_m represent the aperture position error. Then for the i^{th} grid (x_i, y_i) of D, its distance to $\mathbf{a}_m$ in (4) is denoted as $d(m,i) = \sqrt{(x_i - x_m)^2 + (y_i - y_m)^2}$, while the actual one should be:

$$d'(m,i) = \sqrt{(x_i - x_m - \Delta x_m)^2 + (y_i - y_m - \Delta y_m)^2} \quad (6)$$

The divergence between $d(m,i)$ and $d'(m,i)$ will cause error in localization. The measurement matrix $\mathbf{A}$ can be denoted as a function of the aperture position error $\mathbf{e}$, and the localization model (5) is modified as:

$$\mathbf{s} = \mathbf{A}(\mathbf{e})\mathbf{r} + \mathbf{n}, \ \mathbf{e} = [\Delta x_1, \Delta y_1, ..., \Delta x_M, \Delta y_M]^T \quad (7)$$

Accordingly, the solution $\hat{\mathbf{r}}$ of (5) and (7) has only one non-zero element. As a consequence, the problem of localization is transformed into finding a vector $\hat{\mathbf{r}}$ with a single non-zero element which satisfies (5) and (7), and the index i of the non-zero element corresponds to the actual tag position according to (2). Because of noise and multi-path, it is likely that the number of non-zero elements in $\hat{\mathbf{r}}$ is more than one. However, if the direct reflected signal by the interrogated tag plays a dominant role in the received signal for most aperture points, the biggest non-zero element represents the actual tag position, due to the spatial diversity of noise and multi-path. Unless the direct propagation path is blocked, the signal from the direct path is usually much stronger than signals from indirect paths. Finally, the localization problem is transformed into finding the index of the biggest non-zero element in $\hat{\mathbf{r}}$.

III. Detailed Designs of PEC

In this section, the algorithm for synthetic aperture RFID with aperture position error compensation is proposed.

A. Basic Method without Position Compensation

In this subsection, we focus on the simplified localization model (5), where the aperture position error is ignored.

In practical environments, the number M of aperture points in (5) is much less than the number of grids PQ, so (5) has infinite solutions. Fortunately, the prior knowledge that $\mathbf{r}$ has only one non-zero element, can in turn simplify the problem (5) [23]. Due to the sparsity of $\mathbf{r}$, the synthetic aperture RFID localization (5) is a Compressed Sensing (CS) problem:

$$\min_{\mathbf{r}} ||\mathbf{r}||_0, \quad s.t. \ ||\mathbf{A}\mathbf{r} - \mathbf{s}||_2 \leq \epsilon \quad (8)$$

where the sensing matrix $\mathbf{A}$ should satisfy the restricted isometry property (RIP), $\mathbf{r}$ is a k-sparse vector with $k = 1$, and noise $\mathbf{n}$ is bounded with ϵ. If $\mathbf{A}$ satisfies RIP, the number of aperture points must be bigger than $0.28kln(PQ/k)$ with $M \times PQ$ matrix $\mathbf{A}$ (corollary of RIP) [24]. If there are 10000 grids, the minimum number of aperture points is 2.57 or 4.77 when k=1 or k=2, which can be satisfied in most scenarios. According to Lagrange multipliers, (8) can be written as:

$$\mathbf{r} = \arg\min_{\mathbf{r}} \left\{||\mathbf{A}\mathbf{r} - \mathbf{s}||_2^2 + \mu||\mathbf{r}||_0\right\} \quad (9)$$

where μ is the regularization coefficient.

Then we use Stagewise Weak Gradient Pursuit (StWGP) [25] to get the solution of (9). It is an iterative process, and the results ($\mathbf{r}^{[j]}$ and $\mathbf{n}^{[j]}$) of the j^{th} iteration are the approximations of $\mathbf{r}$ and $\mathbf{n}$ in the model (5). It contains two main steps:

In j^{th} iteration, StWGP selects new column vectors of the matrix $\mathbf{A}$ which are not selected in the previous iterations and records selected ones (the index set of these columns is T_j). The stagewise weak selection selects several columns in each iteration, and can reduce the required iterations. The selection is based on both residual $\mathbf{n}^{[j]}$ and the column vector of $\mathbf{A}$:

$$T_j = T_{j-1} \cup \left\{t : \frac{|\mathbf{A}(:,t)^H \mathbf{n}^{[j]}|}{||\mathbf{A}(:,t)||_2} \geq \eta \max_i \frac{|\mathbf{A}(:,i)^H \mathbf{n}^{[j]}|}{||\mathbf{A}(:,i)||_2}\right\} \quad (10)$$

where the weakness parameter $\eta \in (0, 1]$ is chosen to increase iteratively. Then all selected columns are used to construct a

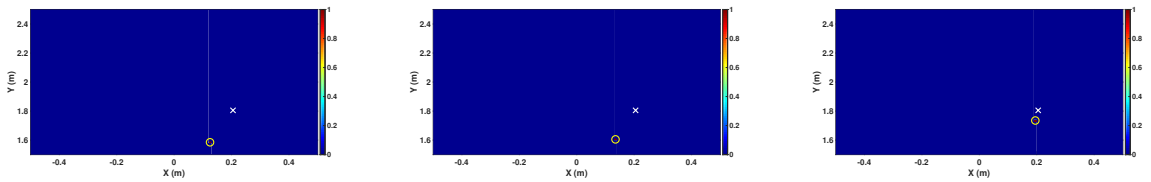

(a) Basic method (0.12 m, 1.58 m). (b) Phase calibration (0.13 m, 1.60 m). (c) PEC (0.19 m, 1.73 m).

Fig. 3. The amplitude of reflection coefficients (**r**) in D after normalization. (The cross represents the actual position (0.20 m, 1.80 m) and the circle represents the estimated position.)

new matrix $\mathbf{A}_{T_j}$. T_j columns of $\mathbf{A}$ form the corresponding columns of $\mathbf{A}_{T_j}$, while other columns of $\mathbf{A}_{T_j}$ are $\mathbf{0}$.

Then we update $\mathbf{r}^{[j]}$ with $\mathbf{r}^{[j-1]}+\alpha\mathbf{d}$, where α is update step size and $\mathbf{d}$ is the update direction $\mathbf{A}_{T_j}^H\mathbf{n}^{[j]}$ (the steepest descent direction of $||\mathbf{s}-\mathbf{A}_{T_j}\mathbf{r}^{[j]}||_2$). StWGP stops when the residual error is smaller than a threshold or the number of iterations reaches a fixed value. Then the position $\mathbf{p}$ corresponding to the maximum $|\mathbf{r}(\hat{i})|$ is regarded as the localization result:

$$i = \arg\max_i |\mathbf{r}(\hat{i})| \tag{11}$$

With the data collected from one typical experiment (22 tag readings and 10000 grids), Fig. 3(a) depicts the amplitude of reflection coefficients (**r**) in D, where the colors of grids denote amplitudes of corresponding reflection coefficients. Due to the prior knowledge that **r** is 1-sparse, we set η to 1 for getting the result with only one iteration. It is apparent that reflection coefficients of most grids are zero (blue), while the grid with non-zero reflection coefficient (red) is near the ground truth.

B. Localization with Phase Calibration

Frequency-dependent $\varphi_{n,\mathrm{r}}$ in (4) needs to be previously measured for every carrier frequency. Fortunately, $\varphi_{n,\mathrm{r}}$ can be simply eliminated for each other with the relative phase. The first reported phase of each carrier frequency $n_{\mathring{m}}$ (at $\mathbf{a}_{\mathring{m}}$) is selected as the reference for others with the same frequency ($n_m = n_{\mathring{m}}$). Then the reported phase φ_m subtracts the corresponding reference phase $\varphi_{\mathring{m}}$. Meanwhile, the ideal phase $4\pi d(m,i)/\lambda_{n_m}$ for each aperture point also subtracts the corresponding one $4\pi d(m,i)/\lambda_{n_{\mathring{m}}}$. The vector **s** and matrix **A** in (5) are modified with the relative phase:

$$\begin{aligned} s(m) &= \exp\{-j(\varphi_m - \varphi_{\mathring{m}})\} \\ a(m,i) &= \exp\left\{-j\frac{4\pi(d(m,i)-d(\mathring{m},i))}{\lambda_{n_m}}\right\} \end{aligned} \tag{12}$$

The StWGP method in Section III-A can still be utilized for (9) with the modified **s** and **A**.

In addition, existing RFID localization systems usually abstract the reader antenna as a point. However, for a practical antenna, its phase center from which radiation emanates to form ideal spherical wave fronts, moves on the evolute of the equiphase wave front [10]. Therefore, the reported phase is AoA-dependent. Different aperture points have different AoAs, which will induce different phase offsets, causing inaccurate localization result. The relative motion between the reader antenna and the tag typically excludes relative rotation, so the tag orientation (relative to the reader antenna) and the polarization mismatch angle are usually stable.

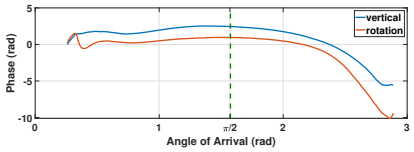

Fig. 4. The AoA response $p(\theta)$ (fitting curve) of reported phase.

We measure this phase offset through a simple experiment with a fixed carrier frequency. In an open space, a static tag is deployed at (0.5 m, 0.13 m), and a reader antenna (transmitting power 24 dBm) moves from (0, 0) to (1.0 m, 0), so the AoA changes from 0.25 rad to 2.89 rad, while tag orientation remains unchanged. At each aperture point, the difference between the reported phase and the corresponding theoretical phase offset φ_{prop}, represents the phase offset due to the reader antenna, the tag and AoA. The first two are constants in this experiment. Therefore, this difference reflects the relationship between the reported phase and AoA. As illustrated in Fig. 4, the phase offset caused by AoA (blue curve) has a broad range. In some situation, this phase offset has little fluctuations. For example, if the tag is at (0.5 m, 2.0 m), its AoA changes from 1.1 rad to 2.0 rad, in which scope the AoA response is stable from Fig. 4.

To calibrate this phase offset, the aforementioned method is utilized to obtain the fitting AoA response curve $p(\theta)$. Then for an aperture point outside the stable scope, all theoretical phase offset φ_{prop} in matrix **A** are corrected by adding $p(\theta)$. Its AoA $\theta(m,i)$ is estimated based on the antenna position $\mathbf{a}_m$ and the tag position $\mathbf{p}$ (corresponding to index i of the vector **r**). So the measurement matrix **A** in (12) is modified as:

$$a(m,i) = e^{-j\left[\frac{4\pi(d(m,i)-d(\mathring{m},i))}{\lambda_{n_m}} + p(\theta(m,i)) - p(\theta(\mathring{m},i))\right]} \tag{13}$$

Then the AoA response of the reported phase is normalized in (13). Although the fitting curve $p(\theta)$ is measured with the unchanged tag orientation, the difference between $p(\theta(m,i))$ and $p(\theta(\mathring{m},i))$ usually remains unchanged due to the static tag with the other tag orientation. For example, if we rotate the tag $\pi/4$ rad, the corresponding $p(\theta)$ (red curve) almost has the same shape as the blue one.

Algorithm 1 Synthetic aperture RFID localization with aperture position error compensation

Input: received signal $\mathbf{s}$, measurement matrix $\mathbf{A}(\mathbf{e})$
Output: reflection coefficient $\mathbf{r}$, aperture position error $\mathbf{e}$

$ir \leftarrow 0$, initialize $\mathbf{e}^{[0]}$ as zero vector
repeat
  $\mathbf{r}^{[ir+1]} \leftarrow \arg\min_{\mathbf{r}} \left\{||\mathbf{A}(\mathbf{e}^{[ir]})\mathbf{r} - \mathbf{s}||_2^2 + \mu||\mathbf{r}||_0\right\}$
  $\mathbf{e}^{[ir+1]} \leftarrow \arg\min_{\mathbf{e}}\{||\mathbf{A}(\mathbf{e})\mathbf{r}^{[ir+1]} - \mathbf{s}||_2^2 + \lambda||\mathbf{e}||_2\}$
  $ir = ir + 1$;
until $||\mathbf{r}^{[ir]} - \mathbf{r}^{[ir-1]}||_2^2/||\mathbf{r}^{[ir-1]}||_2^2 < \epsilon$
return $\mathbf{r}^{[ir]}$, $\mathbf{e}^{[ir]}$

With the same data used in Fig. 3(a), the estimated position is slightly improved to (0.13 m, 1.60 m) as illustrated in Fig. 3(b) after phase calibration, whose estimated phase values are more consistent with the measured ones.

C. Localization with Aperture Position Error Compensation

As aforementioned, aperture position error is unavoidable. This subsection proposes a synthetic aperture RFID localization method with aperture position error compensation.

In the model (5), the measurement matrix $\mathbf{A}$ is determined by the distance between the aperture point and the grid in D, and regarded as known one previously. In consideration of the aperture position error (model (7)), the localization problem (9) becomes a joint optimization one, in which both the tag position and the aperture position error need to be estimated:

$$[\mathbf{r}, \mathbf{e}] = \arg\min_{\mathbf{r},\mathbf{e}} \left\{||\mathbf{A}(\mathbf{e})\mathbf{r} - \mathbf{s}||_2^2 + \mu||\mathbf{r}||_0 + \lambda||\mathbf{e}||_2\right\} \quad (14)$$

We introduce an iterative algorithm to solve this problem: Firstly, we fix the aperture position error $\mathbf{e}$ and estimate the reflection coefficient vector $\mathbf{r}$. Secondly, we estimate the aperture position error $\mathbf{e}$ based on the reflection coefficient vector $\mathbf{r}$ from the first step. Then we upgrade the measurement matrix $\mathbf{A}$ with the new aperture position error $\mathbf{e}$ for the next iteration. This procedure continues until $\mathbf{r}$ has converged. The synthetic aperture RFID localization algorithm flow with aperture position error compensation is shown in Algorithm 1, where ϵ is a threshold.

Given aperture position error $\mathbf{e}$, the first iteration step is a standard CS based synthetic aperture RFID localization problem (9), so it can be solved by StWGP mentioned in Section III-A with the calibration discussed in Section III-B.

In the second iteration step, the aperture position error is the optimization target, and $\mu||\mathbf{r}^{[ir+1]}||_0$ is a constant. Here we deduce the first complex term without the simple $\lambda||\mathbf{e}||_2$. The loss function $L^{[ir+1]}(\mathbf{e}) = ||\mathbf{A}(\mathbf{e})\mathbf{r}^{[ir+1]} - \mathbf{s}||_2^2$ is:

$$L^{[ir+1]}(\mathbf{e}) = \sum_{m=1}^{M} \left| \sum_{i=1}^{PQ} a(m,i)\mathbf{r}^{[ir+1]}(i) - s(m) \right|^2 \quad (15)$$

where $\mathbf{r}^{[ir+1]}(i)$ is the i^{th} element of $\mathbf{r}^{[ir+1]}$ in the ir^{th} iteration. The position error at initial point of the aperture can be considered as 0 due to the relative motion. According to (15) and (12) or (4) (with or without relative phase respectively), the m^{th} measured signal error $L_m^{[ir+1]}$ is only related to the m^{th} aperture error $\mathbf{e}_m = [\Delta x_m, \Delta y_m]^T$:

$$L_m^{[ir+1]}(\mathbf{e}_m) = \left| \sum_{i=1}^{PQ} a(m,i)\mathbf{r}^{[ir+1]}(i) - s(m) \right|^2 \quad (16)$$

Then the loss function (15) can be written as $L^{[ir+1]}(\mathbf{e}) = \sum_{m=1}^{M} L_m^{[ir+1]}(\mathbf{e}_m)$, and the optimization problem in the second iteration step is equivalent to a group of independent optimization problems $m \in [2, M]$:

$$\mathbf{e}_m^{[ir+1]} = \arg\min_{\mathbf{e}_m} L_m^{[ir+1]}(\mathbf{e}_m) \quad (17)$$

This is an unconstrained optimization problem, which can be solved by gradient-based optimization methods, such as the Quasi-Newton method.

The precondition of using this kind of methods is that the gradient can be calculated. The gradient of the loss function $L_m^{[ir+1]}(\mathbf{e}_m)$ with respect to position error $\mathbf{e}_m$ is:

$$\frac{\partial L_m^{[ir+1]}(\mathbf{e}_m)}{\partial \mathbf{e}_m} = \left[\frac{\partial L_m^{[ir+1]}(\mathbf{e}_m)}{\partial \Delta x_m}, \frac{\partial L_m^{[ir+1]}(\mathbf{e}_m)}{\partial \Delta y_m} \right]^T \quad (18)$$

Take Δx_m for example, the first element of the vector in (18) can be calculated based on the chain rule for the derivative of the composition functions:

$$\frac{\partial L_m^{[ir+1]}(\mathbf{e}_m)}{\partial \Delta x_m} = \sum_{i=1}^{PQ} \frac{\partial L_m^{[ir+1]}(\mathbf{e}_m)}{\partial d'(m,i)} \frac{\partial d'(m,i)}{\partial \Delta x_m} \quad (19)$$

The first part of (19) is:

$$\frac{\partial L_m^{[ir+1]}(\mathbf{e}_m)}{\partial d'(m,i)} = 2\Re\left\{ l(m)\mathbf{r}^{[ir+1]*}(i) \frac{\partial a^*(m,i)}{\partial d'(m,i)} \right\} \quad (20)$$

where the function $\Re(x)$ is the real part of x and $l(m)$ is $(\sum_{i=1}^{PQ} a(m,i)\mathbf{r}^{[ir+1]}(i) - s(m))$. The gradient $\partial a^*(m,i)/\partial d'(m,i)$ depends on $a(m,i)$. For $a(m,i) = exp[-j4\pi(d(m,i) - d(\mathring{m},i))/\lambda_{n_m}]$ in (12), we have:

$$\frac{\partial a^*(m,i)}{\partial d'(m,i)} = \frac{j4\pi}{\lambda_{n_m}} \exp\left\{ j\frac{4\pi(d(m,i) - d(\mathring{m},i))}{\lambda_{n_m}} \right\} \quad (21)$$

According to (6), the second part of (19) is:

$$\frac{\partial d'(m,i)}{\partial \Delta x_m} = \frac{\Delta x_m + x_m - x_i}{d'(m,i)} \quad (22)$$

According to (18)-(22), the gradient of the loss function $L_m^{[ir+1]}(\mathbf{e}_m)$ with respect to position error $\mathbf{e}_m$ is achieved, and $\mathbf{e}_m^{[ir+1]}$ in (17) can be solved. So the second iteration step in Algorithm 1 is consequently implemented. In addition, the gradient-based method achieves the unique solution with the 2-norm term $\lambda||\mathbf{e}||_2$.

The Algorithm 1 is an iterative process, and the convergence of the first and the second iteration step is guaranteed by the property of the CS signal recovery and the gradient-based method respectively, so the Algorithm 1 can be convergent [18]. If η in StWGP is set to 1, Algorithm 1 will converge in the first iteration. In order to avoid reaching the local optimum

in early iterations and increasing the chance of trending the global optimum, StWGP (first iteration step) in early iterations should obtain enough non-zero elements in $\mathbf{r}$ ($\eta < 1$ initially). As the iterations (Algorithm 1) progress, a gradually increasing η will ensure that StWGP achieves less non-zero elements in $\mathbf{r}$ to avoid jumping to the worse solution.

Just as existing synthetic aperture RFID localization systems, the computational complexity of PEC depends on the number of aperture points M and the number of grids N' in the zone of possible tag positions. In every iteration of Algorithm 1, all N' grids need to be traversed. The time complexity of StWGP is $O(aMN')$ [25] for $M \times N'$ measurement matrix $\mathbf{A}$, where a is the number of iterations in StWGP, and it is usually small. The time complexity of the gradient-based method (second iteration step) is $O(bMN')$ with b times iterations. In fact, the gradient calculation in the second iteration step is more complex than multiplication in StWGP, and usually b is bigger than a. So the main latency of the system is due to the second iteration step. Fortunately, the second iteration step can be sped up. Due to the sparsity of vector $\mathbf{r}$, most of its elements are zero. Therefore, only the columns in $\mathbf{A}$, which correspond to the non-zero elements of $\mathbf{r}$, are updated for the calculation in the second iteration step. It can greatly decrease the computational burden in the second iteration step. So the time complexity of the second iteration step is $O(bMN'')$, where N'' is the number of non-zero elements of $\mathbf{r}$ and $N'' \ll N'$.

After aperture position error compensation, the amplitude of estimated $\mathbf{r}$ is shown in Fig. 3(c), and the result is (0.19 m, 1.73 m) with only about 7 cm error. With aperture position error compensation, the position around the tag is more likely to produce the signal (phase) $\hat{\mathbf{s}}$ similar to the reported one $\mathbf{s}$, which is selected according to (10).

IV. Evaluation and Analysis

We implement PEC with COTS RFID devices and demonstrate its performance with extensive experiments.

A. Implementation

PEC is implemented with a COTS RFID reader Impinj R420 [26] and a Laird S9025PR antenna [27] without any modification. This RFID reader operates in the frequency range of 920.625-924.375 MHz (16 carrier frequencies) with the reader mode "Dense Mode (M=4)" for the practical industrial settings. We adopt LLRP protocol [28] extended by Impinj to communicate with the reader and obtain the phase report as soon as possible [29]. The system is implemented using C# on a computer equipped with an Intel Core i9-7900X CPU 3.3 GHz and a 16 GByte memory.

As shown in Fig. 5(a), a self-designed robot leverages the SLAM-based (Simultaneous Localization and Mapping) navigation algorithm with a Kinect and its mean localization error is smaller than 10 cm. The robot is programmed to move at the speed of 0.5 m/s. In practice, it is difficult to get the accurate robot position, we also use a linear guide depicted in Fig. 5(b) for accurate aperture position. The Laird antenna

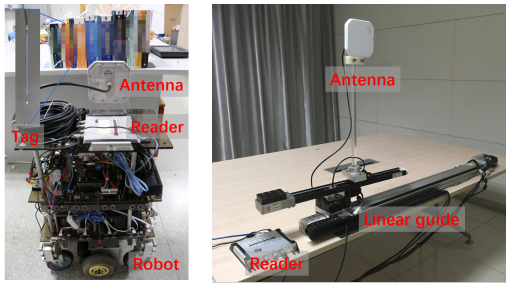

(a) The robot. (b) The linear guide.

Fig. 5. The experiment setup.

is mounted on this equipment with the maximum horizontal moving range of 1 m. This equipment can accurately report its horizontal position in mm-level. We conduct extensive experiments in a typical office room (Fig. 5(a)) and a typical meeting room (Fig. 5(b)) with varying environmental settings, and both scenarios own rich multi-path.

B. Accuracy of PEC

We implement PEC, Tagoram [9] and MobiTagbot [13] with the same hardware shown in Fig. 5 to locate 20 books with library RFID tags for comparison. When the robot moves along the bookshelf (0.5 m apart), the reported phase and the current position of the robot are both recorded.

As mentioned before, the aperture position error will reduce the accuracy of synthetic aperture RFID localization system. The robot moves about 1-1.5 m along the bookshelf, and the tag readings for each tag is about 20-30. After over 100 times experiments, the Cumulative Distributed Function (CDF) of the localization error is illustrated in Fig. 6(a-d), and the spacing of grids is 0.01 m for all systems. As we can see, when the aperture length is 1 m, PEC with aperture position error compensation achieves 5 cm mean error in the lateral direction (parallel to the aperture), outperforming Tagoram, Mobitagbot and PEC without position error compensation by 1.6×, 2× and 1.8× respectively. This improvement gives the credit to the aperture position error compensation and phase calibration. And due to much sparse tag readings, accuracies of Tagoram and Mobitagbot fail to put on a par with their previous results.

In the radial direction (perpendicular to the aperture), PEC still achieves 14 cm mean error, smaller than nearly 20 cm achieved by others. PEC and Mobitagbot leverage multiple carrier frequencies, so they achieve a little higher accuracy in the radial direction. If the relative trajectory has both x-direction and y-direction component, the radial direction accuracy will be much better with more aperture diversity due to the y-direction component of the trajectory [9].

Usually, a longer aperture can improve the localization accuracy of synthetic aperture RFID [10], but at the same time, a bigger accumulated error of AGV position may be also induced. As shown in Fig. 6(c), with the aperture of 1.5 m, the mean error of PEC, Tagoram, Mobitagbot and PEC w.o. is about 4 cm, 7.9 cm, 9 cm and 8.5 cm respectively. Other

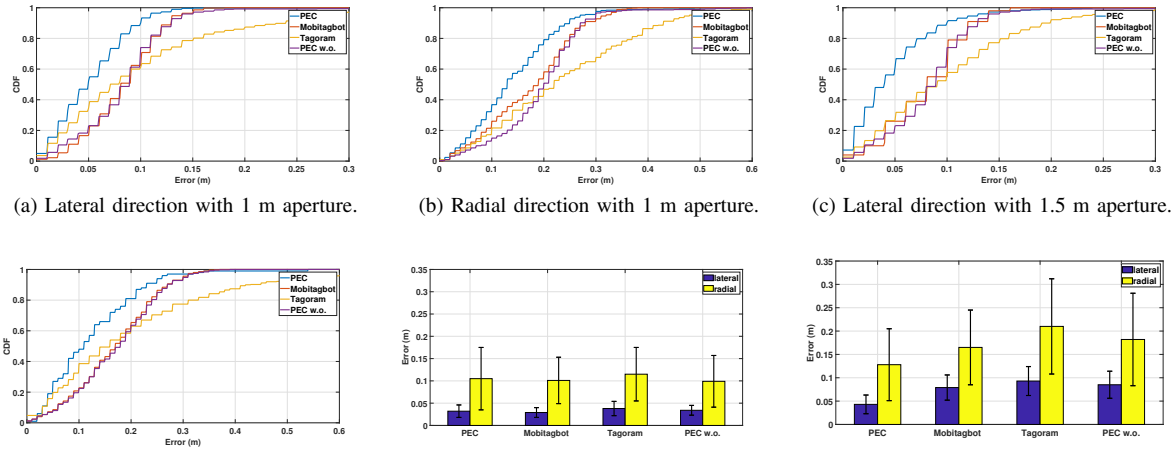

(a) Lateral direction with 1 m aperture. (b) Radial direction with 1 m aperture. (c) Lateral direction with 1.5 m aperture.

(d) Radial direction with 1.5 m aperture. (e) Without aperture position error. (f) With accumulated error (0 at the first aperture point to 0.05 m at the last aperture point).

Fig. 6. Localization error with (a-d, f) or without (e) aperture position error. (PEC w.o. means PEC without position error compensation)

than PEC, their performance improvements are limited. In the radial direction, the accuracy is still dm-level.

We also compare their performance in the controlled scenario with/without aperture position error using the linear guide shown in Fig. 5(b). In each experiment, 10 tags are placed in a row with equal spacing and a fixed distance to the linear guide with 21 equally spaced aperture points. Experiments are repeated for 50 times by arbitrarily changing spacing and distances to collect measurement data, and the results are illustrated in Fig. 6(e)(f). As expected, when there is no aperture position error, these systems achieve similar accuracy. When there is an artificial accumulated error from 0 to 0.05 m along the aperture, only the degradation of PEC is quite limited. This demonstrates the effectiveness and robustness of aperture position error compensation in PEC. Tagoram and MobiTagbot leverage differential augmented hologram with multiple antennas and weight based on entropy to enhance performance respectively. However, they are lack of compensation for the aperture position error.

C. Benchmarks

To further analyze the performance of PEC, several benchmarks are performed.

1) System Latency: To verify the latency of PEC, we run 1000 times simulation with 20 aperture points for a random target tag in 100 $\times$ 100 grids. The simulated aperture positions contain random position error and the measured phase values are all added with Gaussian noise $N(0, 0.1^2)$ [9], [29]. The relationship between the iteration times and the residual error ($||\mathbf{A}(\mathbf{e}^{[ir]})\mathbf{r}^{[ir]} - \mathbf{s}||_2^2$, ir is the ir^{th} iteration) is illustrated in Fig. 7(a). After 2 iterations, the mean residual error converges towards 0. As mentioned in Section III-C, the second iteration step in Algorithm 1 consumes more time, while it can be sped up with less non-zero elements of $\mathbf{r}$. As depicted in Fig. 7(a), the time cost for the first iteration of Algorithm 1 is about 0.5 s on our PC, while it is less than 0.23 s for other iterations. After 2 iterations, the mean error in the lateral direction is smaller than 5 cm, as shown in Fig. 7(b). The mean localization results in both two directions converge at 4 or 5 iterations, so we set the maximum number of iterations to 5 in PEC. Then the total latency is about 1.5 s, which is within an acceptable level for applications with low real-time demand.

2) Phase Calibration: As shown in Fig. 7(c), when we use the proposed iterative algorithm, the mean error without the phase calibration increases by 1.1 cm in the lateral direction compared to that with the phase calibration. In our experiments, AoA changes from $\pi/4$ rad to $3\pi/4$ rad. According to Fig. 4, the corresponding AoA response changes almost 1 rad. Although PEC without phase calibration achieves satisfactory accuracy owing to the effective position error compensation, phase calibration is still necessary to narrow the accuracy gap caused by AoA response of reported phase.

3) Aperture Position Error Compensation: As aforementioned, the performance of synthetic aperture RFID localization depends on the aperture point position accuracy. Based on the linear guide, we add different zero-mean Gaussian noise on the antenna position reported by the linear guide to simulate the aperture point position error. As shown in Fig. 7(d), PEC is robust to the aperture point position error. We also add accumulated error whose value linearly increases to 0.05 m or 0.10 m and results are also depicted in 7(d). The accumulated error is more harmful, but PEC can compensate for the aperture position error effectively. The zero-mean Gaussian noise is incoherent at different aperture points, so the position error compensation of PEC is more effective.

4) Number of Aperture Points: The previous experiments usually have 20 aperture points. It is worth investigating the performance of PEC with more sparse aperture points. Dense tags and a high-speed AGV are common in many scenarios. For the 1 m aperture length in previous book localization experiments, we down-sample the reported phase data to evaluate system performance. As depicted in Fig. 7(e),

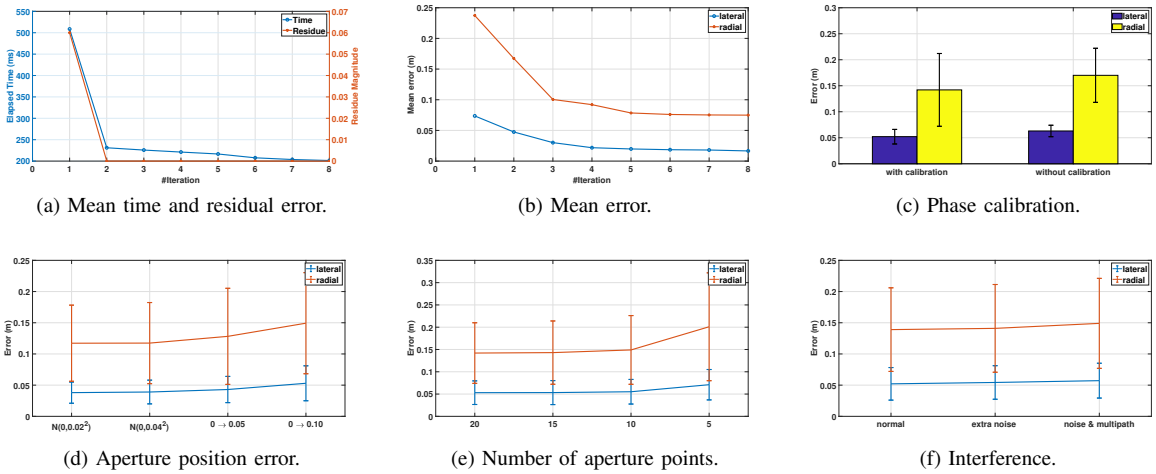

(a) Mean time and residual error. (b) Mean error. (c) Phase calibration.

(d) Aperture position error. (e) Number of aperture points. (f) Interference.

Fig. 7. Several benchmarks for PEC.

PEC with more aperture points has less localization error. By utilizing compressed sensing for localization, PEC can still achieve satisfactory accuracy with few aperture points. Even if there are only 5 aperture points, the mean error is 7 cm and 20 cm in lateral and radial direction respectively. Thus, the number of aperture points is not a crucial factor for our system, and the down-sampling along the aperture can be leveraged to reduce the computational burden.

5) Interference: As aforementioned, the interference such as noise and multi-path distortion can be weakened by each other in coherent reconstruction. It is difficult to carry out a quantitative analysis on the impact, so we utilize an extra reader with ten interference tags in the interrogation zone and two metal reflectors to enhance noise and multi-path distortion respectively. Two metal reflectors are randomly placed, one is near the reader antenna while the other is near tags. As depicted in Fig. 7(f), the accuracy of this situation is almost the same as before. PEC is insensitive to the interference, which is different from one aperture point to another and can be canceled out for each other.

D. Discussion

The proposed method differs from previous synthetic aperture RFID systems in three aspects. First, PEC can effectively handle the gap between the known aperture position and the actual one to achieve the reliable localization result by alternately estimating both the tag position and the aperture position error. Second, the AoA response of the reported phase is normalized in PEC, which can improve the accuracy. Third, PEC leverages compressed sensing and multi-frequency to localize RFID tags, so the interference and noise are further suppressed. Unlike other solutions to (9), such as orthogonal matching pursuit [14], StWGP has much smaller computation burden and fewer iterations. Although the experimental results are promising, PEC still has some limitations. Its latency is a little longer because of heavy computation compared to the state-of-the-art systems. The iterative algorithm could be optimized with some prior knowledge of the aperture position error. In addition, using a 2D aperture with two orthonormal trajectories, better accuracy in the radial direction can be expected.

V. Related Works

Our work is standing on the shoulders of previous works and draws inspiration from them.

A. Phase-based RFID localization

Received signal strength is adopted for localization at first, which is coarse-grained and unstable for RFID. Fortunately, fine-grained phase information reported by modern RFID devices offers opportunities for accuracy localization systems [20], [30]–[35]. However, a higher accuracy usually needs extra cost such as special devices, multiple devices, an extra learning phase and so on. Inspired by the secondary radar, synthetic aperture RFID localization with the inverse correlation filter is proposed [9]–[13]. The relative motion between the reader antenna and the tag construct a virtual antenna array to eliminate position ambiguity caused by the periodicity of reported phase. Existing synthetic aperture RFID localization systems achieve cm-level accuracy with a mobile RFID antenna [9], [10], [13] or a mobile tag [11], [12], [14] or multi-path profiles [15], [16]. In these systems, the hologram is usually used for result representation. However, the difference between the real trajectory (aperture) and the assumed one will lead to localization error due to the inaccurate aperture points in the reconstruction. PEC is inspired by above works but goes further by considering aperture position error compensation.

B. Synthetic Aperture Radar

Based on the prior knowledge of the target scene, compressed sensing is used for SAR imaging [19], [36] with a much lower sampling frequency, but this kind of SAR imaging is a nonlinear reconstruction with a huge computational burden. Due to the individual signal waveform type, compressed

sensing in synthetic aperture RFID localization is different, especially when PEC only needs to get the position of the maximum non-zero reflection coefficient. The motion compensation such as phase gradient autofocus algorithm is common for airborne and spaceborne SAR [17]–[19], but they usually describe the relative motion using a single motion model with determinable parameters or treat the aperture position error as a part of the measured phase error or compensate for phase distortions with burdensome computation. Encouraged by these systems, PEC further develops a COST RFID localization system with aperture position error compensation.

VI. Conclusion

We design and implement PEC, an accurate synthetic aperture RFID localization system with aperture position error compensation. After detailed theoretical analysis, PEC formulates the localization problem as a joint optimization one. It alternately estimates the tag position based on compressed sensing signal recovery and the aperture position error based on the gradient-based optimization method. PEC is also enhanced with the relative phase and phase calibration based on AoA response of reported phase. Extensive experiments with COTS RFID devices prove that the tag position can be estimated accurately with aperture position error. Our future work will focus on higher accuracy in the radial direction, less computational burden and performance improvement with the prior knowledge of the aperture position error.

Acknowledgment

The authors thank the anonymous reviewers for their comments and suggestions. This research was supported by a grant from Shanghai Municipal Commission of Economy and Informatization. Dong Wang is the corresponding author.

References

[1] J. Wang, F. Adib, R. Knepper, D. Katabi, and D. Rus, "Rf-compass: Robot object manipulation using rfids," in *MobiCom*. ACM, 2013, pp. 3–14.

[2] G. Wang, Q. Chen, L. Shangguan, D. Han, J. Han, N. Yang, X. Wei, and J. Zhao, "Hmrl: Relative localization of rfid tags with static devices," in *SECON*, 2017, pp. 1–9.

[3] M. Shneier and R. Bostelman, "Literature review of mobile robots for manufacturing," *National Institute of Standards and Technology, US Department of Commerce*, 2015.

[4] G. N. Desouza and A. C. Kak, "Vision for mobile robot navigation: A survey," *IEEE Transactions on Pattern Analysis & Machine Intelligence*, vol. 24, no. 2, pp. 237–267, 2002.

[5] L. Jia, Z. Feng, W. Yanyan, W. Xia, P. Qingfeng, and C. Lijun, "Rf-scanner: Shelf scanning with robot-assisted rfid systems," in *INFOCOM*. IEEE, 2017, pp. 1–9.

[6] Q. Fan, B. Sun, Y. Sun, and X. Zhuang, "Performance enhancement of mems-based ins/uwb integration for indoor navigation applications," *IEEE Sensors Journal*, vol. 17, no. 10, pp. 3116–3130, 2017.

[7] E. Digiampaolo and F. Martinelli, "A passive uhf-rfid system for the localization of an indoor autonomous vehicle," *IEEE Transactions on Industrial Electronics*, vol. 59, no. 10, pp. 3961–3970, 2012.

[8] S. J. Kim and B. K. Kim, "Dynamic ultrasonic hybrid localization system for indoor mobile robots," *IEEE Transactions on Industrial Electronics*, vol. 60, no. 10, pp. 4562–4573, 2013.

[9] L. Yang, Y. Chen, X.-Y. Li, C. Xiao, M. Li, and Y. Liu, "Tagoram: Real-time tracking of mobile rfid tags to high precision using cots devices," in *MobiCom*. ACM, 2014, pp. 237–248.

[10] R. Miesen, F. Kirsch, and M. Vossiek, "Holographic localization of passive uhf rfid transponders," in *RFID*. IEEE, 2011, pp. 32–37.

[11] A. Parr, R. Miesen, and M. Vossiek, "Inverse sar approach for localization of moving rfid tags," in *RFID*. IEEE, 2013, pp. 104–109.

[12] R. Miesen, F. Kirsch, and M. Vossiek, "Uhf rfid localization based on synthetic apertures," *Automation Science and Engineering, IEEE Transactions on*, vol. 10, no. 3, pp. 807–815, 2013.

[13] L. Shangguan and K. Jamieson, "The Design and Implementation of a Mobile RFID Tag Sorting Robot," in *MobiSys*. ACM, 2016, pp. 31–42.

[14] R. Zhao, Q. Zhang, D. Li, H. Chen, and D. Wang, "Prts: A passive rfid real-time tracking system under the conditions of sparse measurements," *IEEE Sensors Journal*, vol. 18, no. 5, pp. 2097–2106, 2018.

[15] J. Wang and D. Katabi, "Dude, where's my card?: Rfid positioning that works with multipath and non-line of sight," in *SIGCOMM*. ACM, 2013, pp. 51–62.

[16] J. Wang, J. Xiong, H. Jiang, X. Chen, and D. Fang, "D-watch: Embracing bad multipaths for device-free localization with cots rfid devices," in *CoNEXT*, 2016, pp. 253–266.

[17] J. Kirk, J. C., "Motion compensation for synthetic aperture radar," *Aerospace & Electronic Systems IEEE Transactions on*, vol. AES-11, no. 3, pp. 338–348, 1999.

[18] N. Ö. Onhon and M. Cetin, "A sparsity-driven approach for joint sar imaging and phase error correction," *IEEE Transactions on Image Processing*, vol. 21, no. 4, pp. 2075–2088, 2012.

[19] J. Yang, X. Huang, J. Thompson, T. Jin, and Z. Zhou, "Compressed sensing radar imaging with compensation of observation position error," *IEEE Transactions on Geoscience & Remote Sensing*, vol. 52, no. 8, pp. 4608–4620, 2014.

[20] P. V. Nikitin, R. Martinez, S. Ramamurthy, H. Leland, G. Spiess, and K. Rao, "Phase based spatial identification of uhf rfid tags," in *RFID*. IEEE, 2010, pp. 102–109.

[21] GS1 EPCglobal. (2015) Uhf class 1 gen 2 standard. [Online]. Available: https://www.gs1.org/sites/default/files/docs/epc/Gen2_Protocol_Standard.pdf

[22] S. Sen, J. Lee, K.-H. Kim, and P. Congdon, "Avoiding multipath to revive inbuilding wifi localization," in *MobiSys*. ACM, 2013, pp. 249–262.

[23] Y. C. Eldar and G. Kutyniok, *Compressed sensing: theory and applications*. Cambridge University Press, 2012.

[24] E. J. Candes and T. Tao, "Near-optimal signal recovery from random projections: Universal encoding strategies?" *IEEE Transactions on Information Theory*, vol. 52, no. 12, pp. 5406–5425, 2006.

[25] T. Blumensath and M. E. Davies, "Stagewise weak gradient pursuits," *IEEE Transactions on Signal Processing*, vol. 57, no. 11, pp. 4333–4346, 2009.

[26] Impinj. (2018) Speedway r420 rain rfid reader. [Online]. Available: https://www.impinj.com/platform/connectivity/speedway-r420/

[27] Laird. (2018) S9 series - rfid. [Online]. Available: https://www.lairdtech.com/products/s9-series-rfid

[28] GS1 EPCglobal. (2010) Low level reader protocol. [Online]. Available: http://www.gs1.org/sites/default/files/docs/epc/llrp_1_1-standard-20101013.pdf

[29] Impinj. (2013) Application note - low level user data support. [Online]. Available: https://support.impinj.com/hc/en-us/article_attachments/200774268/SR_AN_IPJ_Speedway_Rev_Low_Level_Data_Support_20130911.pdf

[30] L. Shangguan, Z. Zhou, and K. Jamieson, "Enabling gesture-based interactions with objects," in *MobiSys*. ACM, 2017, pp. 239–251.

[31] Y. Bu, X. Lei, L. Jia, B. He, Y. Gong, and S. Lu, "3-dimensional reconstruction on tagged packages via rfid systems," in *SECON*, 2017, pp. 1–9.

[32] L. Shangguan, Z. Yang, A. X. Liu, Z. Zhou, and Y. Liu, "Relative localization of RFID tags using spatial-temporal phase profiling," in *NSDI*, 2015, pp. 251–263.

[33] C. Hekimian-Williams, B. Grant, X. Liu, Z. Zhang, and P. Kumar, "Accurate localization of rfid tags using phase difference," in *RFID*. IEEE, 2010, pp. 89–96.

[34] T. Liu, L. Yang, Q. Lin, Y. Guo, and Y. Liu, "Anchor-free backscatter positioning for rfid tags with high accuracy," in *Proceedings of IEEE INFOCOM*, 2014, pp. 379–387.

[35] L. Yang, Q. Lin, X. Li, T. Liu, and Y. Liu, "See Through Walls with COTS RFID System!" in *MobiCom '15*. ACM, 2015, pp. 487–499.

[36] M. Çetin and W. C. Karl, "Feature-enhanced synthetic aperture radar image formation based on nonquadratic regularization," *IEEE Transactions on Image Processing*, vol. 10, no. 4, pp. 623–631, 2001.